RSC Advances

ROYAL SOCIETY OF CHEMISTRY

www.rsc.org/advances

Journal of Materials Chemistry A

ARTICLE

Multifunctional polymers with biomimetic compound architectures via nanoporous AAO films for efficient solar energy harvesting in dye-sensitized solar cells†

Received 00th January 20xx,
Accepted 00th January 20xx

DOI: 10.1039/x0xx00000x

www.rsc.org/

Bhaskar Dudem,‡[a] Jung Woo Leem,‡[a] Joo Ho Lim,[a] Soo Hyun Lee[a] and Jae Su Yu*[a]

We report the considerable enhancement of the solar power conversion efficiency (PCE) in dye-sensitized solar cells (DSSCs) using a novel biomimetic compound architecture (CA) (i.e., hierarchical nanobumps/microcones arrays)-patterned polydimethylsiloxane (PDMS) with light-harvesting and self-cleaning functions as a protective cover-layer. The CA-patterned PDMS (CA-PDMS) is transferred from a nanoporous anodic alumina oxide mold by facile and cost-effective soft imprint lithography via a microcone-patterned sapphire substrate. A lamination of the CA-PDMS on the glass leads to the increased total and diffuse transmittance properties (i.e., antireflection and light scattering effects), simultaneously, compared to the bare glass over a wide wavelength range of 350-800 nm, exhibiting the much larger solar weighted total transmittance (T_{SW}) value of ~ 94% and average haze ratio (H_A) value of ~ 49.7%, respectively, (i.e., $T_{SW} \approx 90.4\%$ and $H_A \approx 1.4\%$ for the bare glass). In addition, sand dusts on its hydrophobic surface with a water contact angle of ~ 134° are clearly washed by rolling down water droplets (i.e., self-cleaning effect). To simply demonstrate the device applicability, the CA-PDMS is introduced on an outer surface of the front glass substrate in DSSCs. The resulting DSSC with the CA-PDMS exhibits a boosted *PCE* value of ~ 8.24% due to a mainly strong increased short-circuit current density (J_{SC}) value of ~ 18.11 mA cm^{-2} compared to the reference DSSC with the bare glass (i.e., $PCE \approx 7.45\%$ and $J_{SC} \approx 16.37$ mA cm^{-2}) under AM1.5G illumination, indicating the large *PCE* enhancement percentage value of ~ 10.7%.

Introduction

Energy-harvesting techniques from renewable energy resources including solar, wind, biomass, geothermal, tidal, etc., have been an increasing crucial issue to overcome energy crisis, environmental pollution, and global warming throughout the world due to their more extensive exploitation possibility compared to the conventional power supply using fossil fuels.[1-3] Particularly, among these, the solar energy has been considered as an outstanding renewable power source because of its safe, clean (e.g., pollution-, waste-, and noise-free), and unlimitation.[4,5] Its application fields are also very extensive from a small power field such as portable and mobile electronic equipments to large electricity power generating plants. Over the past few years, tremendous efforts have been made to boost the power conversion efficiency (*PCE*) of a dye sensitized solar cell (DSSC) due to its technical feasibility and cost-effectiveness alternative to silicon or III-V material-based solar cells.[6,7] In order to improve the spectral sensitivity and the *PCE* of DSSCs, many studies have been reported on various approaches including optimizing sensitizers,[8] nanostructured active layer itself acts as a scattering layer,[9] photonic crystals,[10] optimizing active layer thickness[11], and increasing the concentration of the attached dye molecules.[12] Additionally, an undyed layer placed on the top of the active layer[13] or a mirror-like Pt counter electrode[14] was also studied as an internal rear reflector. Among various strategies for increasing solar energy harvesting in DSSCs, one simple method is to enhance the light absorption in the active layer of devices over a wide spectral range of the sunlight by introducing an antireflective (AR) and light-scattering layer on the externally facing surfaces of the transparent substrates such as glasses and plastics.[15-19] Recently, for this, biomimetic architectures consisting of nano, micro, or compound (e.g., hierarchical nano/micro configuration) structures have been widely studied in several solar cells.[20-24] Especially, compound structures strongly enhance the optical behaviors (e.g., antireflection, transmission, and diffuse light scattering) of transparent substrates in a wide range of wavelengths and incident angles.[25-29] In the compound architecture (CA), the microstructure extends an optical path of the light and promotes a diffuse light-scattering transmission resulting from higher orders of diffracted waves, while maintaining high total (i.e., specular and diffuse) transmission.[30] On the other hand, the nanostructure with a period smaller than the wavelength of incident light allows for the only zeroth order of the diffracted wave and acts as a homogeneous medium with a gradient-refractive-index (GRIN)

[a] Department of Electronics and Radio Engineering, Kyung Hee University, 1732 Deogyeong-daero, Giheung-gu, Yongin-si 446-701, South Korea. E-mail: jsyu@khu.ac.kr

†Electronic Supplementary Information (ESI) available: SEM image of the Mc-PSS, wetting behavior of the bare glass and the F-PDMS, dynamic wetting behavior of the CA-PDMS at an inclination angle of 40°. See DOI: 10.1039/x0xx00000x

‡These authors contributed equally to this work.

profile between air and the material, thus further effectively suppressing the Fresnel reflection at the surface.[31,32] Therefore, an introduction of the compound structure into the solar cells would lead to the increase of the overall light absorption in the active layer, and thus the solar power generation of DSSCs could be enhanced. However, for the realization of these multi-scale compound structures, complicated and expensive fabrication methods including patterning and etching processes are mostly required, which causes the increase of fabrication cost and time, including a scale limitation.[25-29] A cost-effective, simple, and fast soft imprint lithographic (SIL) patterning method makes it possible to relatively easily form artificial compound structures on the surface of transparent substrates using ultraviolet or thermal curable polymers.[33-36] Although the master molds are also prepared by the lithography patterning and etching processes, once the master molds and the replica polymer stamps are made, they can be repeatedly used for pattern transfers into secondary substrates. Furthermore, the large-scale fabrication techniques (i.e., roll-to-roll and roll-to-plate processes) of master molds and stamps have been developed in the soft imprint lithography,[37] which would facilitate the mass-production for industry applications. In general, a polydimethylsiloxane (PDMS) has been often used to transfer multi-scale patterns precisely on other substrates due to its low free surface energy, flexibility, transparency, and hardness.[33-39] For transparent substrates, the CA-patterned PDMS (CA-PDMS) has the usability since it is not only strongly easy-laminated on a planar surface, but also simply detached from it. Furthermore, as a protective cover-layer, it can improve optical properties of transparent substrates because of its lower refractive index (i.e., $n \approx 1.43$),[40] which could enhance the photo-generated currents in DSSCs. To form a desirable CA-PDMS, the mold with the negatively same compound structure, which is usually prepared by nano- and micro-lithography patterning and etching, is required. Actually, the formation of nanostructures rather than microstructures on the surface of molds gives rise to an increase of fabrication complexity and cost because they can be generally fabricated by expensive electron (e)-beam, nanoimprint, and laser interference lithography or post-heat/chemical treated colloidal spheres and metal nanoparticles with a subsequent dry etching process (e.g., reactive ion etching or inductively coupled plasma etcher system). But, if an electrochemical oxidation process of aluminum (Al) films is employed in a particular acidic electrolyte solution, the nanostructures on microstructured molds can be easily and cost-effectively fabricated without any dry etching processes.[41,42] Meanwhile, self-cleaning properties have been found to be useful in removing any surface pollutants for high-performance devices in practical external applications.[20,33] Thus, the surface wetting behavior of CA-PDMS is also important. Several studies have been reported on the efficient antireflection characteristics of nano, micro, or compound structured polymer films, which were prepared by the SIL method,[34,43,44] as well as the *PCE* improvement of organic and inorganic solar cells by utilizing them on the surface of transparent substrates as a protective cover-layer.[20,33,45,46] However, there is very little or no report on the use of the CA consisting of hierarchical nanostructures on the microstructure arrays at the surface of polymer films as a multifunctional (i.e., light-harvesting and self-cleaning) protective cover-layer of glass substrates in DSSCs using the porous anodic alumina oxide (AAO) templates with a negative CA as a master mold via the SIL. So, it is very meaningful to study the photovoltaic performance of the DSSCs incorporated with compound structured polymer films on the outer glass surface of DSSCs including their optical and surface wetting properties. In this work, we fabricated the artificial biomimetic compound structures consisting of hierarchical nanobumps on microcone arrays at the surface of the PDMS using the SIL via the AAO molds imprinted from the patterned sapphire substrate (PSS) with microcone arrays. The fabricated CA-PDMS was laminated on glass substrates and its optical and self-cleaning behaviors were characterized. For a theoretical analysis of optical light scattering properties, the finite-difference time-domain (FDTD) simulation was also performed. Finally, to simply show the practical feasibility on solar cell devices, the fabricated CA-PDMS was applied into the glass substrate of DSSCs as a protective cover-layer and their device current-voltage (*J-V*) curves and incident photon to current conversion efficiency (*IPCE*) spectra were explored.

Experimental and numerical modelling details

Fabrication of AAO molds

0.25 mm-thick Al sheets (99.999% purity, *Alfa Aesar*) with a size of 3×3 cm^2 were cleaned by an ultra-sonication with acetone, ethanol and de-ionized (DI) water for 10 min, and subsequently dried under a stream of argon. To reduce the surface roughness, the Al sheets were electro-polished in a mixture of perchloric acid and ethanol ($HClO_4$:C_2H_5OH=1:4 in volume ratio) with a voltage of 15 V, which was applied between anode (i.e., Al) and cathode (i.e., platinum, Pt) for 5 min, at an electrolyte temperature of 5 °C. 2D periodic inverted microcone arrays on the surface of the Al sheets (i.e., IMc-Al mold) were formed using a commercial microcone-patterned sapphire substrate (i.e., Mc-PSS), which was fabricated by conventional photolithography and subsequent inductively coupled plasma dry etching process with BCl_3/He mixture gases, purchased from *AND Co.* by an imprinting method with an applied pressure of 25 MPa at a temperature of 210 °C. After that, the IMc-Al molds were anodized in a 3 wt% phosphoric acid (H_3PO_4) solution at 0 °C for 25 min under an applied voltage of 120 V. To widen the pore diameter, the anodized samples were additionally dipped into the 5 wt% H_3PO_4 solution at 30 °C for 8 min, creating the AAO molds with hierarchical inverted nanopores/microcones (compound) architectures (i.e., ICA-AAO molds). On the other hand, the Np-AAO molds with a large pore size were prepared from the electro-polished Al sheets by the same anodization process.

Fabrication of NbA-, McA- and CA-PDMS

A *h*-PDMS solution, which was prepared by mixing VDT-731 (*Gelest, Inc.)* and HMS-301 (*Gelest, Inc.*) copolymers, was

spin-cast on the Np-AAO molds, IMc-Al molds, and ICA-AAO molds, respectively, and then cured at 80 °C for 30 min. Afterwards, a Sylgard 184 (*Dow Corning Co.*) mixed *s*-PDMS solution with a ratio of 10:1 (base:agent) was poured on the corresponding *h*-PDMS/molds, and subsequently cured at 80 °C for 3 h. Finally, the PDMS (*h*-PDMS/*s*-PDMS) were carefully peeled off from the molds, thus producing the NbA-, McA-, and CA-PDMS, respectively.

Preparation of DSSCs

DSSCs with an active area of 0.5×0.5 cm^2 were conventionally fabricated by drop-casting the polymer electrolyte solution onto the photoanode and covering the device with the counter electrode. 15 μm-thick TiO_2 particles (PST-18NR, *CCIC*) were coated on the surface of fluorine doped tin oxide (FTO)-deposited soda lime glasses by using a doctor-blade process using polyimide tapes as the spacer, and then it was heat-treated at 500 ºC for 2 h in a furnace. The TiO_2-coated FTO/glasses were sensitized with ruthenium (II) N719 dye solution (3×10^{-4} M in ethanol, *Solaronix*) for 24 h at room temperature in dark. To prepare a counter electrode, platinum paste (counter PT-1, *Dyesol*) was coated onto FTO/glass with the same doctor-blade method, followed by calcinations at 500 ºC for 2 h. Subsequently, the electrolyte (electrolyte HPE, *Dyesol*) was injected and sealed with the help of a hot press. Finally, the DSSCs were placed in a vacuum oven for one day to completely evaporate the solvent.

Characterized Instrumentation:

The surface morphologies of the fabricated samples were observed by using a SEM (LEO SUPRA 55, *Carl Zeiss*). The optical properties were measured by using a UV-vis-NIR spectrophotometer (Cary 5000, *Varian*) with an integrating sphere at near normal incidence. The water contact angles were measured and averaged at three different positions on the surface of samples by using a contact angle measurement system (Phoenix-300, *SEO Co., Ltd.*) with ~5 μL droplets of DI water. The dynamic advancing and receding water contact angles were also explored on a precise control tilting stage with an inclination angle of 40°. A solar simulator (SUN 3000, *ABET*) with 1000 W Xe short arc lamp and a source meter (Keithley 2400) were used for the *J-V* measurements of the DSSCs. *IPCE* data were obtained by using a 300 W xenon arc lamp as the light source coupled to a monochromater (TLS-300x xenon light source, *Newport*) with optical power meter (2935-c, *Newport*). After calibration using a silicon photodiode (818-UV, *Newport*), the *IPCE* spectra were taken by illuminating monochromatic light on the DSSCs.

Numerical modelling and simulations

The theoretical analysis on optical light scattering behaviors of the different architectures on the PDMS was also carried out using FDTD simulation. To design the theoretical model, in simulations, the hierarchical nanobumps/microcones on PDMS were represented by a periodic geometry in the Cartesian coordinate system by a scalar-valued function of two variables, $f(x, z)$, for simplicity. It was assumed that the incident light enters from air into the structure at normal incidence. The E_y, that is, amplitude of y-polarized electric field, was calculated for the incident plane wave with a slab mode beam profile, which is normalized at λ= 550 nm. For the PDMS film, the refractive index was assumed to be 1.43, and the extinction coefficient was not considered because it is negligible.

Result and discussion

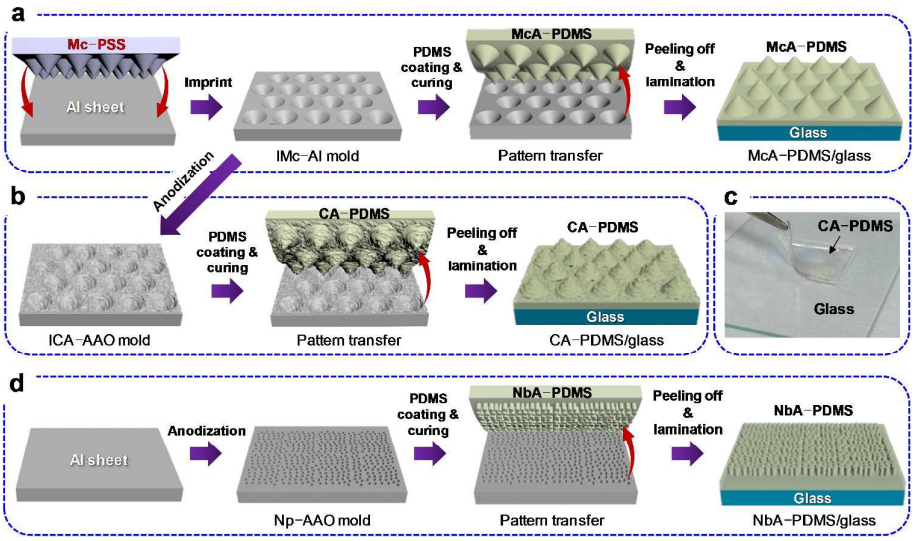

Fig. 1. Schematic diagram of process steps for the fabrication of the PDMS with different architectures via the SIL technique: (a) Microcone architectured PDMS (McA-PDMS), (b) compound architectured PDMS (CA-PDMS), and (d) nanobump architectured PDMS (NbA-PDMS). (c) Photograph for showing the easy lamination and detachability of the CA-PDMS on the flat bare glass.

Fig. 1 illustrates the schematic diagram of process steps for the fabrication of PDMS with different architectures via the SIL technique. Firstly, to fabricate the microcone architecture (McA)-PDMS (Fig. 1(a)), two-dimensional (2D) periodic inverted microcone arrays on the surface of the electro-polished Al sheets (i.e., IMc-Al mold) were formed by pressing the microcone-patterned sapphire substrate (i.e., Mc-PSS), prepared by conventional photolithography and dry etching processes, in an applied pressure of 25 MPa at a temperature of 210 °C. Subsequently, the IMcA-Al mold was anodized at a temperature of 0 °C for 25 min under an applied voltage of 120 V in a 3 wt% phosphoric acid (H_3PO_4) solution (Fig. 1(b)). To further widen the nanopore size, the anodized sample was additionally dipped into the 5 wt% H_3PO_4 solution at 30 °C for 8 min, thus producing the AAO mold consisting of hierarchical nanopores on inverted microcone arrays (i.e., inverted compound architecture; ICA-AAO molds). The AAO mold with nanopores (i.e., Np-AAO mold) was obtained from the electro-polished planar Al sheets by the same anodizing process (Fig. 1(d)). For the pattern transfer into the surface of the PDMS, a hard PDMS (*h*-PDMS) solution was spin-coated on the corresponding molds, and then all the samples were cured at 80 °C for 30 min. After that, a soft PDMS (*s*-PDMS) solution (Sylgard 184) was poured on the *h*-PDMS/mold, followed by a curing at 80 °C for 3 h. Finally, the PDMS (*h*-PDMS/*s*-PDMS) was carefully peeled off from the mold, thus forming the 200 μm-thick PDMS with positive nanobumps, microcones, and nanobumps/microcones (compound) architectures (i.e., NbA-, McA-, and CA-PDMS), respectively. Additionally, the patterned PDMS layers cannot only be easily and strongly laminated on the surface of glass, but also simply separated from it (Fig. 1(c)).

Fig. 2 shows the top- and side-view SEM images of the fabricated molds (a-c) and the PDMS with different architectures (d-f). To obtain the efficient light-harvesting (i.e., antireflection and light scattering) effect, we chose the conical micrograting structure, which has the average diameter, height, and period of 2.7 μm, 1.5 μm, and 2.9 μm, respectively, with 2D periodic hexagonal pattern arrays (see Fig. S1 in the Supporting Information). This microstructure exhibits a strong light scattering in the transmission, while keeping a high total transmission, over a wide wavelength range of 350-800 nm. The detailed optical properties can be found in our previous report.[30] The closely-packed negaive microcone patterns imprinted by the Mc-PSS were relatively well formed on the surface of Al sheets (Fig. 2(a)). The average diameter, depth, and period of the formed IMc-Al mold are approximately 2.35 μm, 1.4 μm, and 2.9 μm, respectively. By anodizing the IMc-Al mold with the following nanopore-widening process, the ICA-AAO mold was obtained (Fig. 2(b)), showing the increased average diameter and depth of 2.45 μm and 1.55 μm, respectively. Meanwhile, the flat AAO mold with randomly distributed nanopores (i.e., Np- AAO mold) was also prepared (Fig. 2(c)) by the same anodization process, exhibiting their average diameter, depth, and period of about 100 nm, 200 nm,

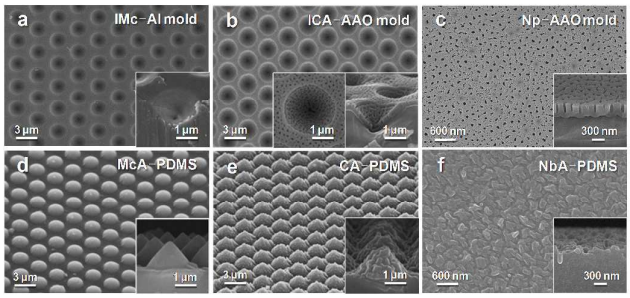

Fig. 2. Top- and side-view SEM images of fabricated molds and samples: (a) IMc-Al mold, (b) ICA-AAO mold, (c) Np-AAO mold, (d) McA-PDMS, (e) CA-PDMS, and (f) NbA-PDMS.

and 180 nm, respectively, and the remaining AAO layer thickness of 100 nm. By using these molds, the positive McA-, CA-, and NbA-patterned PDMS were fabricated by the SIL technique without any large pattern deformations and distortions (Fig. 2(d-f)). Here, it is noteworthy that the CA-PDMS consisting of hierarchical nanobumps/microcones could be easily achieved from the ICA-AAO mold without any expensive and complicated nanolithography processes such as e-beam lithography, nanoimprint lithography, colloidal spheres, metal nanoparticles, etc., for the formation of etching mask nanopatterns. In this experiment, the only Mc-PSS, which can be prepared by a relatively facile, fast, cost-effective, easy-controllable, and large-scale photolithography, was used to form the microstructure. For the resulting McA-PDMS and CA-PDMS, the average diameter and height are 2.35 and 2.45 μm and 1.4 and 1.54 μm, respectively. In contrast, the Np-patterns on the AAO mold with the average depth of ~ 200 nm were poorly transferred on the surface of the PDMS despite the use of the *h*-PDMS. This may be caused by the very small nanopores (i.e., diameter of ~ 100 nm) with the low average period of ~ 180 nm, and thus the *h*-PDMS solution cannot be squeezed into the empty space between the INPs. Consequently, the NbA with a low average depth of ~ 100 nm was formed on the surfaces of both the periodic McA-PDMS (Fig. 2(e)) and flat PDMS (Fig. 2(f)). Nevertheless, the relatively favorable NbA-PDMS, McA-PDMS, and CA-PDMS were fabricated from the corresponding molds by the SIL method, respectively.

The incorporation of the PDMS into the glass clearly improved its transmittance in the wavelength range of 350-800 nm, thus leading to the decreased reflection (Fig. 3(a)). For comparison, the flat PDMS (i.e., F-PDMS) without any patterns was also prepared by the SIL. In Fig. 3(a), the lamination of the F-PDMS on the glass (i.e., F-PDMS/glass) resulted in the slight enhancement of the total transmittance due to the step GRIN profile in the constituent materials of air (n = 1)/PDMS(n ≈ 1.43)/glass (n ≈ 1.53).[30] The patterned PDMS further enhanced the total transmittance of the glass. For the NbA-PDMS/glass, the total transmittance was increased because of a linear GRIN profile between air and the PDMS via the nanobumps. However, at wavelengths of 350-800 nm, its average increment is only

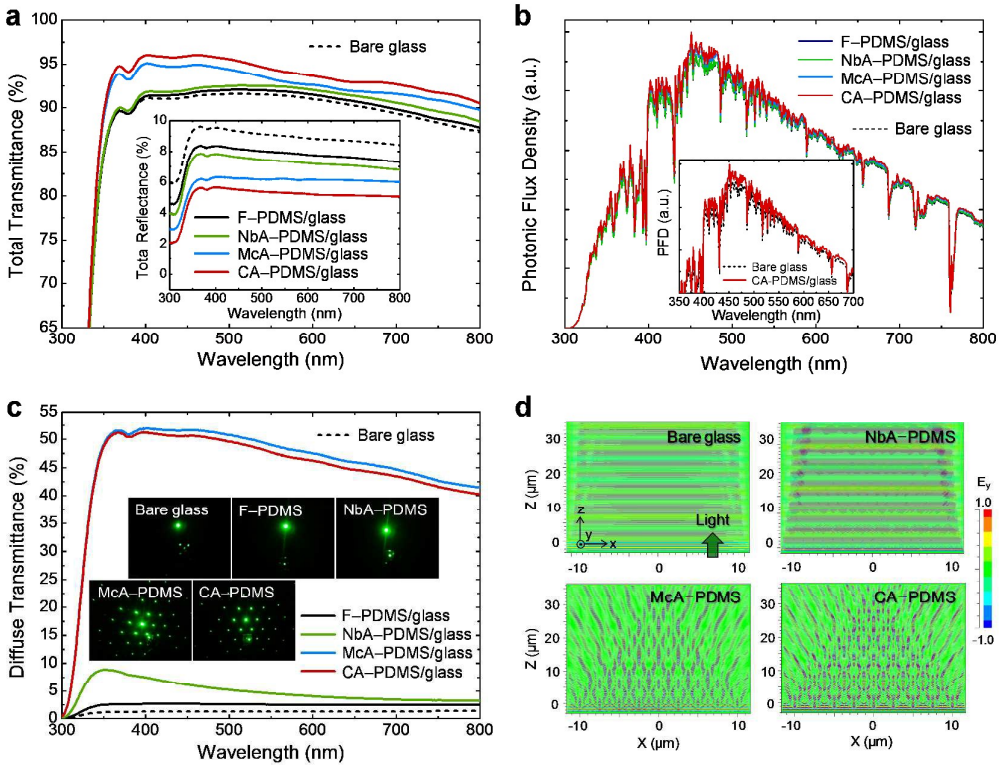

Fig. 3. Measured (a) total and (c) diffuse transmittance spectra of the bare glass, the PDMS with different architectures (F-PDMS, NbA-PDMS, McA-PDMS, and CA-PDMS) including their measured total reflectance spectra in the inset of (a). (b) Spectral distributions of the PFD for their measured total transmittance spectra in (a) and (d) contour plots of E_y distributions for the incident light propagating from air to the corresponding architectured PDMS at λ = 550 nm. Photographs of corresponding samples for the verification of light scattering properties are also shown in the inset of (c).

about 0.6% compared to the F-PDMS/glass since the average arrays not only have a more linear GRIN profile from air to the PDMS due to the larger heights of ≥ 1.4 μm, but also lead to the extension of effective optical path lengths caused by the diffracted and rebounded lights between the microcones,[28,30,49] which can efficiently increase the transmission in transparent materials by reducing the surface reflection. The light scattering properties will be covered in Fig. 3(c). Moreover, for the CA-PDMS, the 180 nm-period nanobumps, which can be regarded as an effective homogeneous medium with a GRIN distribution between air and the bulk PDMS, on microcones allow the only zeroth-order diffracted light to penetrate the PDMS and capture the reflected lights from escaping back to air, thus enhancing the total transmittance (reducing the total reflectance).[47,48] As mentioned earlier, in terms of the reflection (inset of Fig. 3(a)), the CA-PDMS considerably decreased the total reflectance of the glass up to ~ 5% at wavelengths of 350-800 nm. To explore the effect of the transmittance (or reflectance) properties of patterned PDMS as an AR cover-layer on the solar cell performance, the solar weighted transmittance (T_{SW}) (reflectance, R_{SW}), which is the ratio of the usable photons transmitted (reflected) to the total usable photons, was estimated. The T_{SW} (R_{SW}) can be calculated by normalizing the transmittance (reflectance) spectrum with the solar spectral photo flux (i.e., air mass 1.5 global, AM1.5G[50]) integrated over a wavelength range of 350-800 nm.[48] As expected, for the CA-PDMS/glass, the higher (lower) T_{SW} (R_{SW}) value of ~ 94% (~ 5.3%) was obtained compared to the other samples (i.e., T_{SW} ≈ 90.8, 91.4, and 92.9% and R_{SW} ≈ 7.9, 7.3, and 6.2% for the F-PDMS/glass, NbA-PDMS/glass, and McA-PDMS/glass, respectively) as well as the bare glass (i.e., T_{SW} ≈ 90.4% and R_{SW} ≈ 9%).

These transmittance properties at specific wavelengths of solar spectrum can be also observed by the calculation of the photonic flux density (*PFD*) which is the number of photons transmitted across the sample.[51] Fig. 3(b) shows the spectral distributions of the *PFD* for the corresponding samples. Clearly, for the CA-PDMS/glass, the larger *PFD* spectral distribution was shown in a broad wavelength region of 350-800 nm, particularly at wavelengths of 450-550 nm, which is a range of high solar spectral photonic flux intensity, than the other samples. Compared with the bare glass, it also exhibited the much higher *PFD* spectral distribution at wavelengths of 350-800 nm, as shown in the inset of Fig. 3(b). Therefore, it can be

expected that increase of photo-generated currents could be obtained from the cell absorption layer of DSSCs incorporated with the CA-PDMS as a protective AR cover-layer of the glass, so it would lead to the efficiency enhancement of DSSCs.

When the light enters into the grating structure with a period of P at normal incidence, the angle of the transmitted diffraction waves, $\theta_{t,m}$, in the m-th diffraction order is given by the grating equation, $\sin\theta_{t,m} = m\lambda/Pn$,[52] where λ is the incident wavelength of light and n is the refractive index of the incident medium. Therefore, the micro-periodic structures on transparent substrates such as glasses, polymers, etc., have a strong light scattering in transmissions. In addition, the haze ratio (H) is defined by the ratio of the diffuse transmittance (T_d) to the total transmittance (T_t), i.e., $H(\%) = T_d/T_t \times 100$. This H value indicates the light scattering property of a sample. In Fig. 3(c), diffuse transmittance spectra of both the McA-PDMS/glass and CA-PDMS/glass were much larger over a wide wavelength range of 350-800 nm due to their grating period of 2.9 μm while the other samples show almost no diffuse transmittances, exhibiting the average H (H_A) values of ~ 51.4 and ~ 49.7%, respectively (i.e., $H_A \approx 1.4$, 2.8, and 5.3% for the bare glass, F-PDMS/glass, and NbA-PDMS/glass, respectively). This strong light scattering property of both the McA-PDMS and CA-PDMS can be also confirmed from the photographs in the inset of Fig. 3(c). For the flat bare glass, F-PDMS, and NbA-PDMS, there is almost no light diffraction, whearas the McA-PDMS and CA-PDMS show a large diffracted light distribution at λ = 550 nm. Similarly, from the FDTD calculation in Fig. 3(d), the McA-PDMS and CA-PDMS with a period of 2.9 μm exhibit a strong light scattering with a wide angular spread and help a light propagation across the interface between air and the PDMS. For both the flat bare glass and NbA-PDMS, there are no scattered lights. From these results, this strong light scattering effect would positively affect to improve the PCE of DSSCs.[24-26]

The influence of the PDMS with biomimetic architectures as a light-harvesting and protection cover-layer of the outer glass surface on the device performance of DSSCs was studied. The *J-V* curves, the enhancement percentage of device characteristics relative to the reference DSSC, and the *IPCE* spectra for DSSCs with different architectured PDMS cover-layers are shown in Fig. 4(a-c), respectively. Schematic diagram and photograph of the DSSC laminated with the CA-PDMS are shown in the insets of Fig. 4(a) and Fig. 4(c), respectively. For comparison, the *J-V* curve and *IPCE* spectrum of the DSSC with the bare glass as a reference device are also shown in Fig. 4(a) and 4(b), respectively. The device characteristics (open circuit voltage, V_{OC}; short circuit current density, J_{SC}; fill factor, *FF*; *PCE*) of the corresponding DSSCs are summarized in Table 1. The introduction of the patterned PDMS on the external surface of the glass substrate in DSSCs improved the *PCE*. Especially, for the DSSC with the CA-PDMS, the significantly increased *PCE* value of ~ 8.24% was obtained compared to that (i.e., *PCE* ≈ 7.45%) for the reference DSSC, exhibiting the large *PCE* enhancement percentage of ~ 10.7%. This is mainly due to the remarkable enhancement of the J_{SC} value from ~ 16.37 to ~ 18.11 mA cm^{-2} rather than the

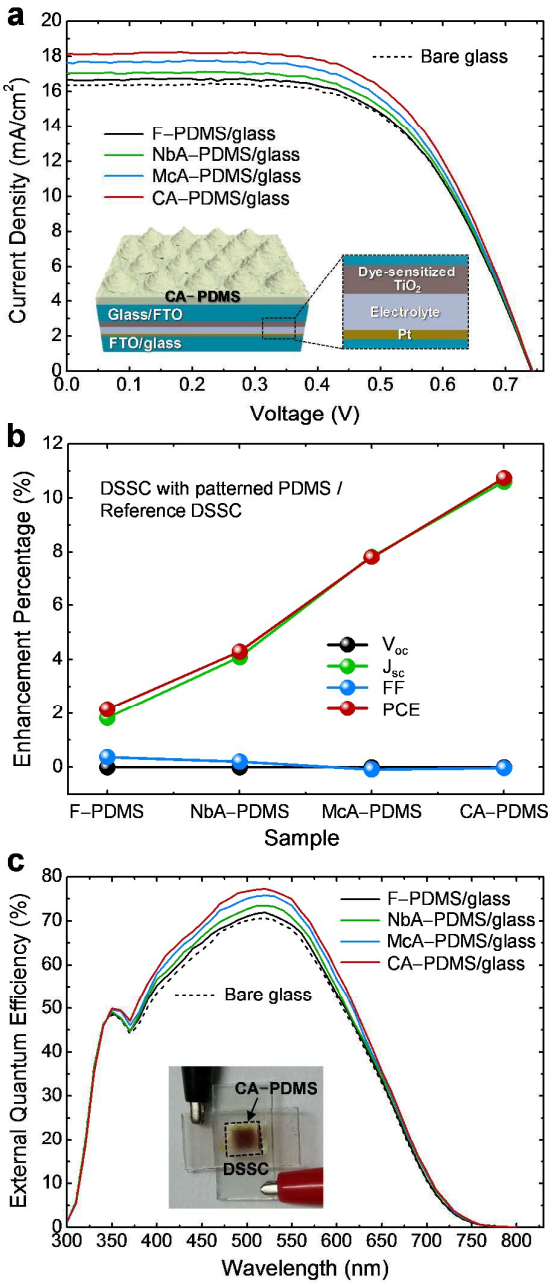

Fig. 4. (a) *J-V* curves, (b) enhancement percentage of device characteristics relative to the reference DSSC, and (c) *IPCE* spectra for DSSCs with different architectured PDMS cover-layers. Schematic diagram and photograph of the DSSC laminated with the CA-PDMS are shown in the insets of (a) and (c), respectively.

V_{OC} and *FF*, as can be seen in Table 1 and Fig. 4(b), because of the higher total transmittance (superior AR ability) and strong light scattering effect over a wide wavelength range of 350-800 nm. This confirms that the efficient light-harvesting layer can boost the light absorption in DSSCs, which produces the

TABEL 1. Device characteristics of DSSCs with different architectured PDMS cover-layers.

[a]DSSC	V_{oc} [V]	J_{sc} [mA cm^{-2}]	FF [%]	PCE [%]
Bare	[b]0.742±0.001	16.37±0.21	61.33±1.05	7.45±0.02
F-PDMS	0.742±0.001	16.67±0.20	61.56±1.00	7.61±0.03
NA-PDMS	0.742±0.001	17.04±0.18	61.46±1.02	7.77±0.06
MA-PDMS	0.742±0.001	17.65±0.22	61.28±1.01	8.00±0.05
CA-PDMS	0.742±0.001	18.11±0.19	61.30±1.06	8.24±0.04

[a]For each DSSC, five devices or more were fabricated in the same fabrication facilities. All the DSSCs were characterized by solar simulator under 1-sun AM1.5G illumination. [b]Mean value ± standard deviation.

improved photocurrents. On the other hand, for all the DSSCs, there is no considerable discrepancy in both the V_{OC} and *FF*. This indicates that the lamination of the PDMS layer does not affect the electrical and material properties in DSSCs. This increased photocurrent can be also observed from the *IPCE* data (Fig. 4(c)). The DSSC with the CA-PDMS showed a higher *IPCE* spectrum than those of the other DSSCs over an entire spectral range of 350-750 nm, indicating the average increment of ~ 10% compared to the reference DSSC at the corresponding wavelengths. This value is similar to the J_{SC} enhancement percentage of ~ 10.6% in the *J-V* characteristics of Table 1.

In outdoor environments, the dust particles and contaminants on the surface of solar cell systems are very harmful and degrade the device performance since they interfere with the incident light into the cell absorption layer. Therefore, the self-cleaning function at the top surface of solar cells is very useful to keep the device performance.[33,53] The water wetting behaviors of PDMS with different architectured surfaces were investigated in Fig. 5. In the photographs of Fig. 5(a), the patterned PDMS showed higher water contact angle (θ_C) values compared to those of the F-PDMS (i.e., $\theta_C \approx 98°$) as well as the bare glass (i.e., $\theta_C \approx 37°$) (see Fig. S2(a) of the Supporting Information), indicating the hydrophobic surface. This is attributed to the increased surface roughness of PDMS explained by the Cassie and Baxter theory.[54,55] In particular, the CA-PDMS exhibited a larger θ_C value of ~ 134° than those of NbA-PDMS ($\theta_C \approx 104°$) and McA-PDMS ($\theta_C \approx 108°$). The air is trapped in the interstices of the rough surface, and thus it can prevent the intrusion of water droplet into the nanobumps/microcones, resulting in the enhancement of the water contact angle on the larger roughened surface of the CA-PDMS. The dusts and pollutants on the hydrophobic surface of the CA-PDMS with the $\theta_C \approx 134°$ can be washed by rainwater droplets because it has relatively large dynamic advancing (θ_{AC}) and receding (θ_{RC}) water contact angle values of $\theta_{AC} \approx 160°$ and $\theta_{RCA} \approx 102°$ at the inclination angle of 40°, respectively, exhibiting the contact angle hysteresis (i.e., $\theta_{AC}-\theta_{RC}$) of ~ 58° (see Fig. S2(b) in the Supporting Information). The self-cleaning behavior of the CA-PDMS is observed in the Fig. 3(b). When the water droplets on the surface of the CA-PDMS covered with sand dusts were dropped, the dusts were clearly

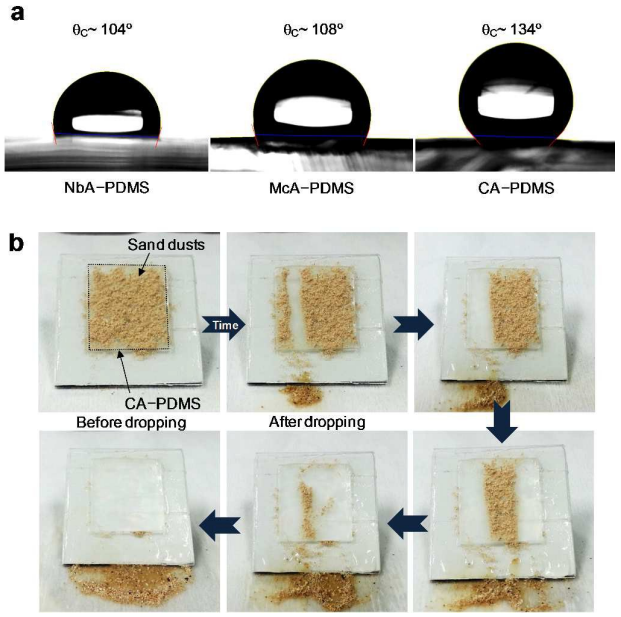

Fig. 5. (a) Photographs of a water droplet on the surface of the NbA-PDMS, the McA-PDMS, and the CA-PDMS. (b) Sequential photographs of water droplet cleaning behaviors for the CA-PDMS.

removed with rolling down water droplets without any remaining sand and water droplets at its surface. Thus, the protective cover-layer with an additional self-cleaning function like this CA-PDMS would enhance its practical feasibility in real outdoor applications including solar cells, displays, windows of buildings or cars, and various other optical components.

Conclusions

The PDMS with the biomimetic compound architecture consisting of hierarchical nanobumps/microcone arrays (i.e., CA-PDMS) was fabricated using the ICA-AAO mold by the SIL technique via the Mc-PSS. For the CA-PDMS/glass, optical and surface wetting behaviors were investigated, together with the theoretical analysis using the FDTD method. It exhibited much higher total and diffuse transmittance characteristics (i.e., $T_{SW} \approx 94\%$ and $H_A \approx 49.7\%$) than those (i.e., $T_{SW} \approx 90.4\%$ and $H_A \approx 1.4\%$) of the bare glass in the broad wavelength range of 350-800 nm, and thus the surface reflection was reduced (i.e., $R_{SW} \approx 5.3\%$). Furthermore, its self-cleaning effect (cf., $\theta_C \approx 134°$ at the inclination angle of 0°, $\theta_{AC} \approx 160°$ and $\theta_{RC} \approx 102°$ at 40°, respectively) was also verified by the removal of sand dusts through the rolling down water droplets. For the DSSC employed with the CA-PDMS as a protective light-harvesting cover-layer of the outer glass substrate, the improved *PCE* value of ~ 8.24% was achieved by the enhanced photo-generated carriers of $J_{SC} \approx 18.11$ mA cm^{-2}, indicating the significant *PCE* enhancement percentage of ~ 10.7% compared to the reference DSSC with the bare glass

(i.e., *PCE* ≈ 7.45%, J_{SC} ≈ 16.37 mA cm^{-2}). These results can offer a deep understanding of biomimetic compound architectured polymers, which can be easily realized by a simple and cost-effective SIL via the AAO mold, with broadband light-harvesting and self-cleaning functions for high-efficiency DSSC device applications. Also, it is important to note that these CA-patterned polymers can be applied to various other solar cells and optic systems that use transparent substrates and covers such as glasses, plastics, sapphires, and quartzes.

Acknowledgements

This work was supported by the National Research Foundation of Korea (NRF) grant funded by the Korea government (MSIP) (No. 2014-069441).

References

1 N. L. Panwar, S. C. Kaushik, S. Kothari, *Renew. Sust. Energ. Rev.,* 2011, **15**, 1513-1524.
2 N. S. Lewis, *Science*, 2007, **315**, 798-801.
3 M. E. Himmel, S. Y. Ding, D. K. Johnson, W. S. Adney, M. R. Nimlos, J. W. Brady, T. D. Foust, *Science*, 2007, **315**, 804-807.
4 M. S. Dresselhaus, I. L. Thomas, *Nature*, 2001, **414**, 332-337.
5 S. Mekhilef, R. Saidur, A. Safari, *Renew. Sust. Energ. Rev.,* 2011, **15**, 1777-1790.
6 U. Bach, D. Lupo, P. Comte, J. E. Moser, F. Weissortel, J. Salbeck, H. Spreitzer, M. Gratzel, *Nature*, 1998, **395**, 583-585.
7 A. Hagfeldt, G. Boschloo, L. Sun, L. Kloo, H. Pettersson, *Chem. Rev.,* 2010, **110**, 6595-6663.
8 N. Robertson, *Angew. Chem. Int. Ed.,* 2006, **45**, 2338-2345.
9 J. Lee, M. Lee, *Adv. Energy Mater.*, 2014, **4**, 1300978.
10 S. Colodrero, A. Mihi, L. Haggman, M. Ocana, G. Boschloo, A. Hagfeldt, H. Miguez, *Adv. Mater.* 2009, **21**, 764-770.
11 K. Zhu, N. R. Neale, A. Miedaner, A. J. Frank, *Nano Lett.,* 2007, **7**, 69-74.
12 M. Pazoki, P. W. Lohse, N. Taghavinia, A. Hagfeldt, G. Boschloo, *Phys. Chem. Chem. Phys.,* 2014, **16**, 8503-8508.
13 S. Ito, S. M. Zakeeruddin, R. H. Baker, P. Liska, R. Charvet, P. Comte, M. K. Nazeeruddin, P. Pechy, M. Takata, H. Miura, S. Uchida, M. Gratzel, *Adv. Mater.*, 2006, **18**, 1202-1205.
14 N. N. Zhang, B. Zhang, Y. H. Li, Y. Hou, S. Yang, J. H. Zhong, H. G. Yang, *J. Mater. Chem. A,* 2014, **2**, 1641-1646.
15 Y. M. Song,; J. H. Jang, J. C. Lee, E. K. Kang, Y. T. Lee, *Sol. Energy Mater. Sol. Cells,* 2012, **101**, 73-78.
16 H. K. Raut, S. S. Dinachali, Y. C. Loke, R. Ganesan, K. K. Ansah-Antwi, A. Gora, E. H. Khoo, V. A. Ganesh, M. S. M. Saifullah, S. Ramakrishna, *ACS Nano*, 2015, **9**, 1305-1314.
17 Y. Nasuno, N. Kohama, K. Nishimura, T. Hayakawa, H.Taniguchi, M. Shimizu, *Appl. Phys. Lett.*, 2006, **88**, 071909.
18 K. Choi, S. H. Park, Y. M. Song, Y. T. Lee, C. K. Hwangbo, H. Yang, H. S. Lee, *Adv. Mater.,* 2010, **22**, 3713-3718.
19 K. C. Park, H. J. Choi, C. H. Chang, R. E. Cohen, G. H. McKinley, G. Barbastathis, *ACS Nano,* 2012, **6**, 3789-3799.
20 S. Y. Heo, J. K. Koh, G. Kang, S. H. Ahn, W. S. Chi, K. Kim, J. H. Kim, *Adv. Energy Mater.,* 2014, **4**, 1300632.
21 Q. Lin, S. F. Leung, L. Lu, X. Chen, Z. Chen, H. Tang, W. Su, D. Li, Z. Fan, *ACS Nano,* 2014, **8**, 6484-6490.
22 Y. Liu, A. Das, S. Xu, Z. Lin, C. Xu, Z. L. Wang, A. Rohatgi, C. P. Wong, *Adv. Energy Mater.,* 2012, **2**, 47-51.
23 J. W. Leem, J. S. Yu, D. H. Jun, J. Heo, W. K. Park, *Sol. Energy Mater. Sol. Cells,* 2014, **127**, 43-49.
24 B. Janthong, Y. Moriya, A. Hongsingthong, P. Sichanugrist, M. Konagai, *Sol. Energy Mater. Sol. Cells,* 2013, **119**, 209-213.
25 H. P. Wang, T. Y. Lin, M. L. Tsai, W. C. Tu, M. Y. Huang, C. W. Liu, Y. L. Chueh, J. H. He, *ACS Nano*, 2014, **8**, 2959-2969.
26 C. H. Ho, D. H. Lien, H. C. Chang, C. A. Lin, C. F. Kang, M. K. Hsing, K. Y. Lai, J. H. He, *Nanoscale,* 2012, **4**, 7346.
27 J. W. Leem, M. S. Kim, J. S. Yu, *J. Opt. Soc. Am. B,* 2013, **30**, 1665-1670.
28 Y. M. Song, G. C. Park, S. J. Jang, J. H. Ha, J. S. Yu, Y. T. Lee, *Opt. Express*, 2011, **19**, A157-A165.
29 J. W. Leem, Y. M. Song, J. S. Yu, *Nanoscale*, 2013, **5**, 10455-10460.
30 Y. H. Ko, J. S. Yu, *Opt. Express,* 2011, **19**, 15574-15583.
31 W. Stork, N. Streibl, H. Haidner, P. Kipfer, *Opt. Lett.,* 1991, **16**, 1921-1923.
32 E. E. Perl, W. E. McMahon, R. M. Farrell, S. P. DenBaars, J. S. Speck, J. E. Bowers, *Nano Lett.,* 2014, **14**, 5960-5964.
33 Y. B. Park, H. Im, M. Im, Y. K. Choi, *J. Mater. Chem.,* 2011, **21**, 633-636.
34 R. J. Martin-Plama, C. G. Pantano, A. Lakhtakia, *Nanotechnology,* 2008, **19**, 355704.
35 N. Koo, M. Bender, U. Plachetka, A. Funchs, T. Wahlbrink, J. Bolten, H. Kurz, *Microelectron. Eng.,* 2007, **84**, 904-908.
36 S. H. Lee, J. W. Leem, J. S. Yu, *Opt. Express,* 2013, **21**, 29298-29303.
37 S. H. Ahn, L. J. Guo, *ACS Nano,* 2009, **3**, 2304-2310.
38 Y. M. Song, Y. Xie, V. Malyarchuk, J. Xiao, I. Jung, K. J. Choi, Z. Liu, H. Park, C. Lu, R. H. Kim, R. Li, K. B. Crozier, Y. Huang, J. A. Rogers, *Nature*, 2013, **497**, 95-99.
39 T. W. Odom, J. C. Love, D. B. Wolfe, K. E. Paul, G. M. Whitesides, *Langmuir,* 2002, **18**, 5314-5320.
40 S. Al-Maawali, J. E. Bemis, B. B. Akhremitchev, R. Leecharoen, B. G. Janesko, G. C. Walker, *J. Phys. Chem. B,* 2001, **105**, 3965-3971.
41 C. Goh, K. M. Coakley, M. D. McGehee, *Nano Lett.,* 2005, **5**, 1545-1549.
42 F. Buyukserin, M. Aryal, J. Gao, W. Hu, *Small* 2009, **5**, 1632-1636.
43 F. Galeotti, F. Trespidi, G. Timo, M. Pasini, *ACS Appl. Mater. Interfaces*, 2014, **6**, 5827-5834.
44 D. H. Ko, J. R. Tumbleston, K. J. Henderson, L. E. Euliss, J. M. DeSimone, R. Lopez,; E. T. Samulski, *Soft Matter,* 2011, **7**, 6404-6407.
45 J. W. Leem, X. Y. Guan, M. Choi, J. S. Yu, *Sol. Energy Mater. Sol. Cells*, 2015, **134**, 45-53.
46 J. K. Hyun, C. Ahn, H. Kang, H. J. Kim, J. Park, K. H. Kim, C. W. Ahn, B. J. Kim, S. Jeon, *Small,* 2013, **9**, 369-374.
47 Y. M. Song, H. J. Choi, J. S. Yu, Y. T. Lee, *Opt. Express,* 2010, **18**, 13063-13071.
48 J. W. Leem, Y. Yeh, J. S. Yu, *Opt. Express*, 2012, **20**, 4056-4066.
49 J. Zhao, M. A. Green, *IEEE Trans. Electron Dev.,* 1991, **38**, 1925-1934.
50 NREL's Renewable Resource Data Center, retrieved 2014, http://rredc.nrel.gov/solar/spectra/am1.5.
51 J. W. Leem, J. S. Yu, *Mater. Sci. Eng. B,* 2011, **176**, 1207-1212.
52 E. Hecht, Optics, 4th ed.; Addison Wesley: San Francisco, CA, 2002.
53 J. Son, S. Kundu, L. K. Verma, M. Sakhuja, A. J. Danner, C. S. Bhatia, H. Yang, *Sol. Energy Mater. Sol. Cells,* 2012, **98**, 46-51.
54 A. B. D. Cassie, S. Baxter, *Trans. Faraday Soc.*, 1994, **40**, 546-551.

55 A. D. Tserepi, M. E. Vlachopoulou, E. Gogolides, *Nanotechnology,* **2006**, *17*, 3977-3983.

Graphical Abstract

Polydimethylsiloxane with a biomimetic compound architecture (i.e., CA-PDMS) consisting of hierarchical nanobumps/microcone arrays with light-harvesting (i.e., antireflection and light scattering) and self-cleaning functions as a protective cover-layer of dye-sensitized solar cells (DSSCs) generates the improved solar power conversion efficiency.